

# Stereoscopic Image Stitching via Disparity-Constrained Warping and Blending

Xiaoting Fan, Jianjun Lei, *Senior Member, IEEE*, Yuming Fang, *Senior Member, IEEE*,  
Qingming Huang, *Fellow, IEEE*, Nam Ling, *Fellow, IEEE*, and Chunping Hou

**Abstract**—As a significant branch of virtual reality, stereoscopic image stitching aims to generating wide perspectives and natural-looking scenes. Existing 2D image stitching methods cannot be successfully applied to the a stereoscopic image without considering the disparity consistency of stereoscopic images. To address this issue, this paper presents a stereoscopic image stitching method based on disparity-constrained warping and blending, which could avoid visual distortion and preserve disparity consistency. First, a point-line-driven homography based disparity minimization method is designed to pre-align the left and right images and reduce vertical disparity. Afterwards, a multi-constraint warping is proposed to further align the left and right images, where the initial disparity map is introduced to control the consistency of disparities. Finally, a disparity consistency seam-cutting and blending method is presented to determine the optimal seam and conduct stereoscopic image stitching. Experimental results demonstrate that the proposed method achieves competitive performance compared with other state-of-the-art methods.

**Index Terms**—Stereoscopic image, image stitching, disparity consistency, multi-constraint warping, seam-cutting and blending

## I. INTRODUCTION

WITH the rapid development of multimedia and display techniques, stereoscopic image processing has become a hot research topic. Furthermore, as important and effective scene representations of virtual reality, stereoscopic images are key components for creating interactive virtual scenes [1]-[3]. At present, in order to obtain a stereoscopic image with a wide perspective, the mainstream method focuses on stitching a number of left and right images, which are obtained by a high-resolution double-view camera [4]-[6]. However, the inconsistencies in object positions in the left and right images may cause visual fatigue and influence stereoscopic perception. Therefore, ensuring that the stereoscopic image

Manuscript received August, 2018. This work was supported in part by the National Key R&D Program of China (No. 2017YFB1002900), National Natural Science Foundation of China ( No. 61722112, 61520106002, 61620106009, U1636214 ), and Natural Science Foundation of Tianjin (No. 18ZXZNGX00110, 18JCJQJC45800). (Corresponding author: J. Lei)

X. Fan, J. Lei, and C. Hou are with the School of Electrical and Information Engineering, Tianjin University, Tianjin 300072, China (e-mail: xtfan@tju.edu.cn; jjlei@tju.edu.cn; hcp@tju.edu.cn).

Y. Fang is with the School of Information Management, Jiangxi University of Finance and Economics, Nanchang 330032, China (e-mail: fa0001ng@e.ntu.edu.sg).

Q. Huang is with the School of Computer Science and Technology, University of Chinese Academy of Sciences, Beijing 101408, China, and also with the Key Laboratory of Intelligent Information Processing, Institute of Computing Technology, Chinese Academy of Sciences, Beijing 100190, China (e-mail: qmhuang@ucas.ac.cn).

N. Ling is with the Department of Computer Engineering, Santa Clara University, Santa Clara, CA 95053 USA (e-mail: nling@scu.edu).

has a reasonable disparity range and that the stitched image has less visual distortion are challenging issues in stereoscopic image stitching.

For 2D image stitching, some homography-based methods [7]-[11] have been proposed to warp and stitch the images. In these methods, a homography matrix is mainly designed to solve the problems of perspective distortion and shape distortion. In addition, in order to improve the poor correspondences of low-texture regions, the content-preserving warping is introduced in some studies [12]-[14]. In these studies, the image is first divided into uniform dense grid mesh. Then, mesh-based warping and optimization are conducted by adding global similarity prior or local similarity transformation to obtain more accurate alignment. Finally, the overlapping regions of the warped images are blended to obtain a smooth seamless stitched image.

Compared with traditional 2D image stitching technologies, an effective stereoscopic image stitching method needs to not only avoid perspective and shape distortions but also guarantee the disparity consistency of stereoscopic images [15], [16]. Therefore, some 2D image stitching methods have been extended to achieve stereoscopic image stitching and improve stereoscopic perception. Tang *et al.* [17] proposed a content-based 3D stitching representation for long video sequences of dynamic urban scenes. In [18], a solution for generating high-quality stereo panoramas at mega pixel resolutions was presented and a flow-based up-sampling was used to resolve the issue of stitching artifacts. Peleg *et al.* [19] proposed two optical omnistereo panorama systems to capture images from different viewpoints. The left and right panorama can be stitched by taking multiple strips from a camera. However, these methods do not consider the disparity constraint in the whole process of stereoscopic image stitching.

In this paper, we propose a stereoscopic image stitching method based on disparity-constrained warping and blending. The main contributions of this paper are summarized as follows.

- 1) A disparity-constrained warping and blending method for stereoscopic image stitching is proposed in this study, in which the disparity constraint is proposed to guide the whole stereoscopic image stitching.
- 2) Considering that the vertical disparity can be controlled by feature points in the homography coordinate, a point-line-driven homography based disparity minimization method is designed to pre-align left and right images and reduce vertical disparity.
- 3) In order to align the left and right images more accurately and further preserve disparity information, a multi-

constraint warping method is presented to reduce shape distortion and eliminate disparity artifacts.

- 4) To blend aligned left and right images and avoid disparity distortions, a disparity consistency seam-cutting and blending method is exploited to determine the optimal seam and stitch stereoscopic images.

The rest of this paper is organized as follows. Section II gives a brief overview of related work. Section III presents the proposed stereoscopic image stitching method. Experimental results and analysis are reported in Section IV. The paper is concluded in Section V.

## II. RELATED WORK

In this section, we review two key points of existing image stitching methods, i.e., homography-based warping [20] and seam-cutting and blending [21], [22].

### A. Homography based warping

Some pioneering works of image stitching methods employed single global homography with parametric transforms to conduct image stitching [23], [24]. These methods used invariant local features to select matching images and construct homography, which is applied to establish mapping relations in order to align images. To enhance the alignment ability, two homographies are introduced to align the background and foreground to achieve seamless stitching results [25]. Lin *et al.* [26] proposed an image stitching method with a smoothly varying affine field, which can retain the good extrapolation of parametric transforms. Those global homography models are flexible to handle image stitching under the condition without obvious disparity changing. However, the images taken from non-planar or discontinuous surfaces scenes cannot be well processed.

In order to solve the issues of global homography, some composite image stitching techniques have been proposed. Zaragoza *et al.* [27] proposed the milestone method named As-Projective-As-Possible (APAP) which learns the warp based on moving Direct Linear Transformation (DLT). Based on APAP, line correspondences in the modified DLT framework is extended in [28], which can provide stronger correspondences. In [29], Chang *et al.* introduced a method which can extrapolate the projective transformation of overlapping regions into non-overlapping regions and gradually change from projective to similarity across the image. Lin *et al.* [30] presented a method which can reduce the perspective distortion in non-overlapping regions by linearizing homography and slowly change it to global similarity. These efforts cause a more adaptive stitching than global homography, as images are divided into dense cells and a local homography is applied to each transformed dense cell for accurate alignment.

Inspired by the local homography method, many content-aware or content-preserving warping methods are introduced into image stitching [31], [32]. Chen *et al.* proposed an image stitching method with the global similarity prior, so that the results look as natural as possible [33]. In [34], [35], feature lines are adopted as alignment constraint and imposed to the content-preserving warping framework to reduce

alignment errors and preserve image structures. Xiang *et al.* [36] presented a two-stage warping-based model by imposing additional feature lines correspondences, which are adopted as another structure constraint for image stitching. However, these methods do not consider the blending optimization of the warped images, which would cause ghosting artifacts.

### B. Seam-cutting and blending

Seam-cutting and blending methods, such as image retargeting [37], video blending [38], and image stitching [39], have been widely applied in image editing. The seam-cutting and blending method used in image stitching is mainly employed to search a high-quality seam, which is further used to blend images. Zhang *et al.* [14] developed a seam finding method that estimates a plausible seam from aligned images by considering both global geometric alignment and image content. In [40], the estimated seam is deployed to guide the operation of optimizing local alignment so that the seam quality gets improved at each iteration. Li *et al.* [41] proposed a perception-based energy function in the seam-cutting framework, which considers the nonlinearity of human perception in energy minimization. However, traditional image editing techniques cannot be directly used in stereoscopic image stitching, as disparity distortions would lead to a poor visual experience or misleading depth information in stereoscopic images. Therefore, many efforts have been devoted to preserve disparity consistency recently. Zhang *et al.* [42] manipulated a casual stereoscopic panorama stitching method, in which the target disparity map is optimized to avoid vertical disparity and the seam-cutting is formulated as a labeling problem solved by a graph-cut method. In [43], a content-preserving warping was introduced to locally refine alignment and an extended seam-cutting method was applied to find a seam in the aligned image. These methods can reduce visual fatigue and retinal rivalry effectively. However, in these above methods, the feature points are insufficient or unreliable for image matching, which would lose rich correspondences for accurate warping model estimation. Additionally, the disparity constraint is applied to a certain process in stereoscopic image stitching, instead of being applied to supervise the whole image stitching process.

In this paper, a disparity-constrained warping and blending method is proposed for stereoscopic image stitching. In the proposed method, a point-line-driven homography is designed by considering feature points and feature lines, and a disparity minimization function is employed to reduce vertical disparity. Meanwhile, a novel multi-constraint warping with disparity map is proposed to locally refine the pre-aligned left and right images and eliminate artifacts caused by disparity inconsistency. Furthermore, a disparity constrained seam-cutting and blending method is introduced to find smoothing seams and fuse images while considering the disparity consistency. Extensive evaluation on public datasets shows that the proposed method performs better than the existing ones.

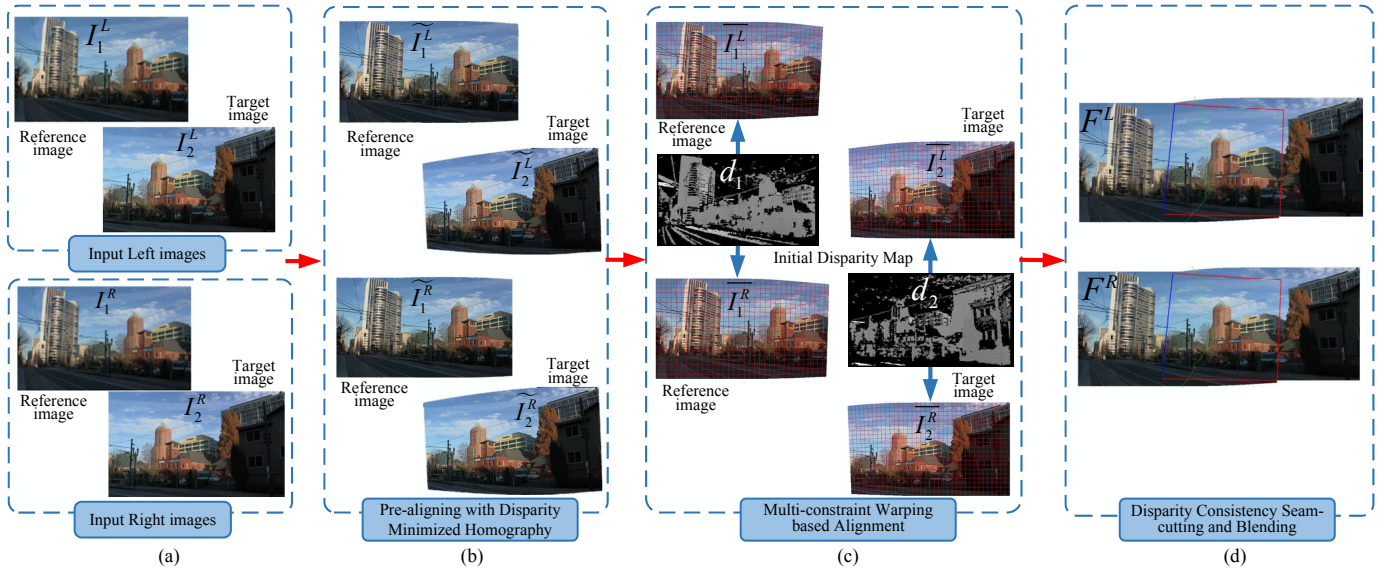


Fig. 1. The flowchart of the proposed method.

### III. PROPOSED STEREOSCOPIC IMAGE STITCHING METHOD

#### A. Framework overview

The proposed stereoscopic image stitching method consists of three parts, including pre-aligning with disparity minimized homography, multi-constraint warping based alignment, and disparity consistency seam-cutting and blending, as shown in Fig. 1. First, feature points and feature lines are extracted as key characteristics of the input left images ( $I_1^L, I_2^L$ ) and right images ( $I_1^R, I_2^R$ ), where the point-line-driven homography based disparity minimization method is deployed to pre-align the input left and right images. Afterwards, as the pre-aligned left images ( $\tilde{I}_1^L, \tilde{I}_2^L$ ) and right images ( $\tilde{I}_1^R, \tilde{I}_2^R$ ) might still be misaligned, the multi-constraint warping with the help of disparity map ( $d_1, d_2$ ) is employed to further adjust the disparity and fine-tune image structures. Finally, the disparity consistent seam-cutting and blending method is manipulated to fuse the aligned left images ( $\bar{I}_1^L, \bar{I}_2^L$ ) and right images ( $\bar{I}_1^R, \bar{I}_2^R$ ). The final stitched images are represented as ( $F^L, F^R$ ).

#### B. Pre-aligning with disparity minimized homography

Compared with 2D images, stereoscopic images contain disparity information of scenes. Thus, the homography used in traditional 2D image stitching cannot be directly applied to stereoscopic image stitching. Therefore, a disparity minimized homography is proposed to pre-align left and right images. Given that the vertical disparity of a stereoscopic image can be controlled by feature points [44] in the spatial coordinates, the vertical disparity constraints of the transformed target left and right images are calculated to minimize the differences between the y-coordinates of the feature points after pre-aligning. Moreover, some significant information of image structures may be lost when the homography is only estimated from feature points. Thus, feature lines [45] are introduced as another matching clue to obtain the disparity minimized homography. Based on the above analysis, the optimized

homographies  $H_L$  and  $H_R$  for target left and right images are determined as follows.

$$H_L^* = \arg \min_{H_L} \left( \sum_{i=1}^{N_L} \|p_i'^L - H_L p_i^L\|^2 + \sum_{m=1}^{\rho_L} \|(l_m'^L)^T H_L l_m^L\|^2 + \sum_{k=1}^{N_O} |[H_L p_k'^{OL}]_y - [H_R p_k'^{OR}]_y|^2 \right) \quad (1)$$

$$H_R^* = \arg \min_{H_R} \left( \sum_{j=1}^{N_R} \|p_j'^R - H_R p_j^R\|^2 + \sum_{n=1}^{\rho_R} \|(l_n'^R)^T H_R l_n^R\|^2 + \sum_{k=1}^{N_O} |[H_L p_k'^{OL}]_y - [H_R p_k'^{OR}]_y|^2 \right) \quad (2)$$

where  $i, j$  and  $k$  denote the indexes of matched feature points;  $m$  and  $n$  represent the indexes of matched feature lines;  $N_L, N_R$  and  $N_O$  denote the number of matched feature points;  $\rho_L$  and  $\rho_R$  denote the number of matched feature lines;  $(p_i^L, p_i'^L)$  and  $(l_m^L, l_m'^L)$  are the matched feature points and feature lines of  $(I_1^L, I_2^L)$ ;  $(p_j^R, p_j'^R)$  and  $(l_n^R, l_n'^R)$  are the matched feature points and feature lines of  $(I_1^R, I_2^R)$ ;  $p_k'^{OL}$  represent the matched feature points in the overlapping region of  $(I_1^L, I_2^L)$ ; and  $p_k'^{OR}$  denote the matched feature points in the overlapping region of  $(I_1^R, I_2^R)$ .  $[H_L p_k'^{OL}]_y$  and  $[H_R p_k'^{OR}]_y$  are the y-coordinates of feature points after transformation of target left and right images. Since the above functions are least squares problems, DLT [27] is adopted to solve the energy functions to obtain the optimal homographies  $H_L$  and  $H_R$ .

After calculating the energy functions, the pre-aligned target left and right images ( $\tilde{I}_1^L, \tilde{I}_2^L$ ) are obtained based on the transformation of the disparity minimized homographies. To further reduce global alignment distortions, global warping is designed to pre-align the reference images. Considering vertical disparity is easily generated when warping the reference image, a vertical disparity constraint is introduced in the

global warping. Simultaneously, a global similarity constraint is used to preserve the global image structures. The global warpings,  $S_L$  and  $S_R$  for the reference left and right images are expressed as follows.

$$S_L^* = \arg \min_{S_L} \left( \sum_{i=1}^{N_L} \|S_L p_i^L - p_i'^L\|^2 + \sum_{k=1}^{N_O} |[S_L p_k'^{OL}]_y - [S_R p_k'^{OR}]_y|^2 \right) \quad (3)$$

$$S_R^* = \arg \min_{S_R} \left( \sum_{j=1}^{N_R} \|S_R p_j^R - p_j'^R\|^2 + \sum_{k=1}^{N_O} |[S_R p_k'^{OR}]_y - [S_L p_k'^{OL}]_y|^2 \right) \quad (4)$$

where  $i$  and  $j$  are the indexes of matched feature points;  $[S_L p_k'^{OL}]_y$  and  $[S_R p_k'^{OR}]_y$  are the y-coordinates of feature points after transformation of reference left and right images. Warping the reference image using the global warping could cause misalignment of the overlapping region between reference and target images. We coordinate the warping of the reference image by using the solved disparity minimized homography. The final transformation of the reference image can be obtained as  $G = S(H)^{-1}$ , where  $S$  is the global warping and  $H$  is the disparity minimized homography.

Fig. 2 visually compares samples of the disparity minimized homography with and without disparity constraint. From the first two rows, it can be seen that there are no obvious visual differences in image stitching results between these two cases. However, it can be seen from Fig. 2(c) that the stereoscopic image without disparity constraint produces obvious vertical disparity (see the enlarged red and yellow boxes), which leads to retinal rivalry and disparity artifacts. In contrast, the proposed method with disparity constraint generates a better stereoscopic image with fewer vertical disparities (see the enlarged red and yellow boxes in Fig. 2(f)).



Fig. 2. Visual comparison samples of disparity minimized homography. From top to bottom: the stitched left images, the stitched right images, and the red-cyan anaglyph of stereoscopic image. (a)-(c) are stitched images without disparity constraint in disparity minimized homography. (d)-(f) are stitched images with disparity constraint in disparity minimized homography.

### C. Multi-constraint warping based alignment

After the pre-aligning processing, there remain some misalignments and incorrect vertical disparities. In order to further preserve disparity consistency and eliminate shape distortion, a multi-constraint warping based alignment method is proposed in this section. Inspired by the content-preserving method based on mesh warping, the image warping is expressed as a grid-mesh warping problem, in which the coordinates of the grid-mesh vertexes are unknown. Furthermore, the warping problem is formulated as a quadratic minimization issue, which considers the differences between the coordinates of feature points on the mesh vertexes. Therefore, an objective energy function is defined to estimate the grid-mesh vertexes of aligned images. In addition, a stereoscopic disparity constraint is constructed to preserve the disparity consistency of stereoscopic images. The multi-constraint warping includes three constraints, i.e., a stereoscopic disparity constraint, a global similarity constraint, and a smoothness constraint. Thus, the total energy function  $E$  is defined as:

$$E(\bar{v}) = E_d(\bar{v}) + E_g(\bar{v}) + E_s(\bar{v}) \quad (5)$$

where  $E_d$  represents stereoscopic disparity constraint;  $E_g$  represents global similarity constraint; and  $E_s$  represents smoothness constraint.  $\bar{v} = \{\bar{v}_p\}$  denotes the unknown set of grid mesh in the aligned left and right images.

According to the characteristics of the human vision system, the disparity map can provide shared depth information of important objects in the left and right scenes. Therefore, the initial disparity map is utilized in the stereoscopic disparity constraint to ensure the disparity of the aligned images close to that of the original images. In our method, the stereoscopic disparity constraint includes a horizontal disparity constraint and a vertical disparity constraint. The horizontal disparity constraint is applied to control the generated depth perception and preserve the original perceived depth distribution. The vertical disparity constraint is employed to reduce vertical disparity after warping and prevent visual fatigue. The stereoscopic disparity constraint  $E_d$  is defined as:

$$E_d(\bar{v}) = (E_d(\bar{v})_x + E_d(\bar{v})_y)/2 \quad (6)$$

where  $E_d(\cdot)_x$  is the horizontal disparity constraint;  $E_d(\cdot)_y$  is the vertical disparity constraint.

For the horizontal disparity constraint, to guarantee that the horizontal disparity of the aligned left and right images is close to the original horizontal disparity, the horizontal disparity constraint  $E_d(\cdot)_x$  is given as:

$$E_d(\bar{v})_x = \sum_{p=1}^{n_p} \|[\bar{v}_p^L]_x - [\bar{v}_p^R]_x - d(\bar{v}_p)\|^2 \quad (7)$$

where  $p$  is the index of matched feature points;  $n_p$  represents the number of vertexes with convincing feature points;  $[\bar{v}_p^L]_x$  and  $[\bar{v}_p^R]_x$  are the  $x$ -coordinates of vertex sets in the aligned left and right images; and  $d(\bar{v}_p)$  is the disparity value.

The vertical disparity constraint is applied to minimize the difference between the  $y$ -coordinates of the mesh vertex in the

aligned left and right images. Therefore, the vertical disparity constraint  $E_d(\cdot)_y$  is defined as:

$$E_d(\bar{v})_y = \sum_{p=1}^{n_p} \|[\bar{v}_p^L]_y - [\bar{v}_p^R]_y\|^2 \quad (8)$$

where  $[\bar{v}_p^L]_y$  and  $[\bar{v}_p^R]_y$  are the  $y$ -coordinate of vertexes sets in the aligned left and right images.

In addition, a global similarity constraint is introduced to ensure the regions without feature correspondences of the aligned image are as consistent as possible with the pre-aligned image, and the smoothness constraint is applied to keep the aligned images as smooth as possible. The definitions of these two constraints are similar to those in [42].

The total objective energy function (5) can be minimized by a linear least-squares function solver, and the output grid-mesh can be obtained using the bilinear interpolation method. Fig. 3 shows some visual comparison samples of multi-constraint warping based alignment with and without disparity constraint. The first two rows show that multi-constraint warping without a disparity constraint can also achieve global alignment with few shape distortions. However, the comparison results of the stereoscopic images in Figs. 3(c)-(f) show that the vertical disparity is obviously reduced by the stereoscopic disparity constraint (see the enlarged red and yellow boxes), which prevents ambiguities and disparity distortions.

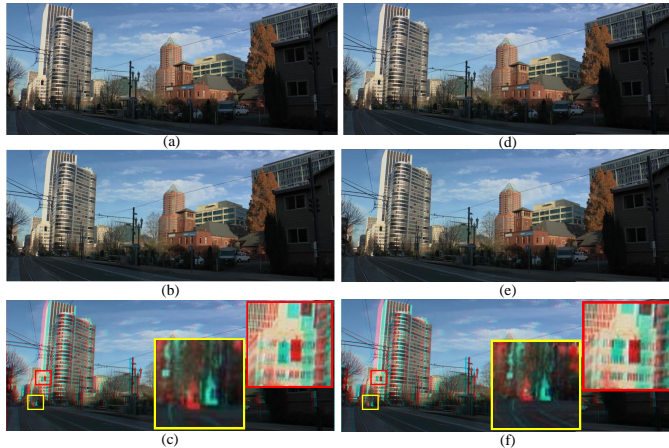


Fig. 3. Visual comparison samples of multi-constraint warping based alignment. From top to bottom: the stitched left images, the stitched right images and the red-cyan anaglyph of stereoscopic image. (a)-(c) are stitched images without disparity constraint in multi-constraint warping. (d)-(f) are stitched images with disparity constraint in multi-constraint warping.

#### D. Disparity consistency seam-cutting and blending

In order to eliminate artifacts generated by local misalignment in the stitched image, a disparity consistency seam-cutting and blending method is proposed to obtain the final stitched stereoscopic image. In general, the traditional seam-cutting method is applied to find a seam with minimal differences between the two images by constructing a data term and a smoothness term. However, this does not consider the disparity information between left and right images when compositing stereoscopic image. Therefore, in our method, a

disparity constraint is introduced into the seam-cutting method to preserve the disparity consistency of stereoscopic images. The disparity consistency term, data term, and smoothness term are jointly considered, and the energy function  $E_{seam}$  is defined as:

$$E_{seam}(l) = E_{dis}(l) + E_{data}(l) + E_{smo}(l) \quad (9)$$

where  $E_{dis}$  represents the disparity consistency term;  $E_{data}$  represents the data term; and  $E_{smo}$  represents the smoothness term.

For the disparity consistency term, we hope the disparity of each pixel in or around the seam in the aligned reference images is close to that in the aligned target images. Assuming the overlapping region of two aligned images is defined as a set, we assign each pixel  $s$  in the set a label  $l_s$  with a value of either 1 or 2, where '1' corresponds to  $\bar{I}_1$  and '2' corresponds to  $\bar{I}_2$ . If two adjacent pixels  $s$  and  $t$  in the set take different labels, the disparity difference between  $\bar{I}_1$  and  $\bar{I}_2$  should be as small as possible along the seam. The disparity consistency term is formulated as a labeling problem:

$$E_{dis}(l) = \sum_{s,t} ((K(s, \bar{I}_1^L, \bar{I}_1^R, \bar{I}_2^L, \bar{I}_2^R) + K(t, \bar{I}_1^L, \bar{I}_1^R, \bar{I}_2^L, \bar{I}_2^R))|l_s - l_t|) \quad (10)$$

$$K(s, \bar{I}_1^L, \bar{I}_1^R, \bar{I}_2^L, \bar{I}_2^R) = |\bar{I}_1^L(s) - \bar{I}_1^R(s)| - |\bar{I}_2^L(s) - \bar{I}_2^R(s)| \quad (11)$$

where  $s$  and  $t$  are the adjacent pixels in the overlapping region of two aligned images;  $(l_s, l_t)$  is a pair of labels to a pair of pixels  $(s, t)$ . Additionally, the data term and smoothness term are calculated as the same with the study [41].

In order to solve the energy function  $E_{seam}$ , the graph-cut max-flow method [46] is implemented to find a high-quality seam that satisfy the minimum seam-cutting energy function between the two images. Meanwhile, multi-band blending [47] is employed to reduce misalignments in the stitched images and eliminate seam discontinuity. Through the above steps, the stitched left and right images ( $F^L, F^R$ ) are obtained and applied to the composite stereoscopic image.

Fig. 4 gives some visual comparison samples of seam-cutting and blending with and without the disparity constraint. It can be seen from Fig. 4(c) that the vertical disparity is obvious in the stereoscopic image due to the lack of a disparity consistency term. In contrast, the vertical disparity is reduced and the horizontal disparity is preserved by applying the additional disparity constraint (see the enlarged red box in Fig. 4(f)).

## IV. EXPERIMENTAL RESULTS AND ANALYSIS

### A. Experimental Setup

To demonstrate the effectiveness of the proposed method, quantitative and qualitative experiments are conducted in this study. Two datasets are used in the experiments. The first dataset [42] is composed of 21 stereoscopic images and the second dataset [43] is composed of 6 stereoscopic images. However, it is difficult to obtain all the corresponding results from the comparison methods, so 10 stereoscopic images,

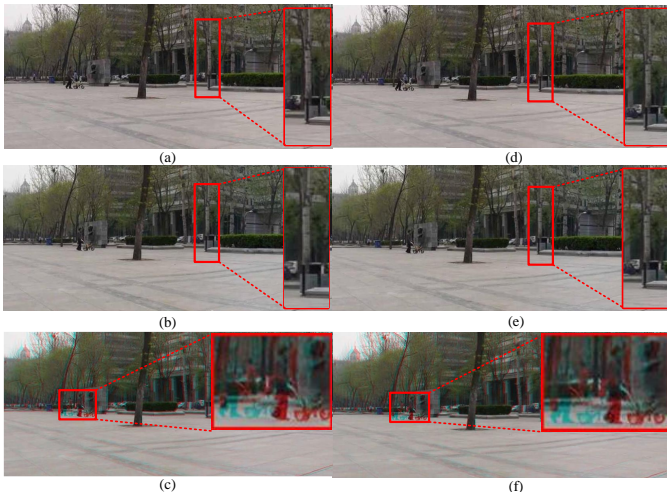


Fig. 4. Visual comparison samples of disparity consistency seam-cutting and blending. From top to bottom: the stitched left images, the stitched right images, and the red-cyan anaglyph of stereoscopic image. (a)-(c) are stitched images without disparity constraint in seam-cutting. (d)-(f) are stitched images with disparity constraint in seam-cutting.

Flowerpot, House, Umbrella, Sculpture, Lake, Office Building, Alocasia, White Building, Flower, Panorama, are used in the comparison experiments. Quantitative evaluation of the stereoscopic image stitching involves two important evaluation measures. The first is average absolute vertical disparity (AVD) [43], which is defined as follows.

$$AVD = \frac{\sum_{h=1}^H |vd_h|}{H} \quad (12)$$

where  $|vd_h|$  denotes the absolute vertical disparity of the  $h$ -th feature point; and  $H$  denotes the total number of feature points. The smaller vertical disparity is, the better 3D viewing experience achieves.

In addition, the average gradient (AG) is used to evaluate whether an image is smooth and free of ghosting [48]. A higher AG means a higher-quality stitched result. The formulation is defined as follows.

$$AG = \frac{1}{MN} \sum_{i=0}^{M-1} \sum_{j=0}^{N-1} \sqrt{[(\frac{\partial Y(i,j)}{\partial x})^2 + (\frac{\partial Y(i,j)}{\partial y})^2]^{\frac{1}{2}}} \quad (13)$$

where  $Y(i,j)$  is the gray value of  $(i,j)$ ;  $M$  and  $N$  are the total numbers of rows and columns in an image, respectively.

## B. Comparison Results

1) *Visual Comparison*: In this section, we compare the proposed method with four state-of-the-art methods, i.e., APAP [27], AANAP [30], CSPS [42], and HWM [43]. APAP and AANAP are 2D image stitching methods, while CSPS and HWM are designed for stereoscopic image stitching. It is worth noting that the results of APAP are obtained by running the public source code; the results of AANAP are obtained through our own implementation; and the results of CSPS and HWM are obtained from the authors.

Fig. 5 shows the comparison results between the proposed method and APAP. It can be seen that the left and right images

obtained by APAP have obvious distortions. For example, the pillar in the overlapping region suffering from severe bending (see the enlarged yellow boxes in Fig. 5(c)). In contrast, thanks to the accurate alignment and the optimized seam-cutting scheme, the proposed method provides satisfactory image stitching performance with fewer artifacts (see the enlarged pillar regions in Fig. 5(d)). Moreover, from the stereoscopic image results shown in the third row of Fig. 5 (see the enlarged red boxes in Fig. 5(c)), APAP would cause obvious vertical disparity, which leads to inconsistent stereoscopic perception. In contrast, the proposed method (see the enlarged red boxes in Fig. 5(d)), which considers the disparity consistency constraint, not only obtains a better stereoscopic image but also reduces shape distortion.

Fig. 6 shows the comparison results of the proposed method and AANAP. As an improvement of the traditional APAP, AANAP achieves desirable results in 2D image stitching as shown in the first two rows of Fig. 6(c). However, due to the lack of a disparity constraint in stereoscopic image stitching, AANAP cannot completely eliminate the vertical disparity or effectively preserve the horizontal disparity (see the red box in the third row of Fig. 6(c)). By contrast, the proposed method obtains better stereoscopic image results (see the red box in Fig. 6(d)). The integration of alignment warping and the disparity constraint not only reduces the vertical disparity but also preserves the original horizontal disparity.

To further verify the performance of the proposed method, the other two stereoscopic image stitching methods (i.e., CSPS and HWM) are used for comparison in Figs. 7 and 8. CSPS also considers the role of the target disparity map in stereoscopic image stitching. Therefore, a satisfactory stereoscopic image with fewer vertical disparities is obtained, as shown in Fig. 7 (see the third row in Fig. 7(c)). However, some shape distortions exist in both left and right images. As shown in Fig. 7, the original shapes of the objects in the final stitched images are not preserved and there exist some visual distortions. For instance, the stone tablet and parterre (see the red boxes in the image in Fig. 7(c)) have obvious enlargement and tilting. However, our method better preserves the proportions of objects and better avoids distortions (see the red boxes in the Fig. 7(d)). The main reason is that, with the help of multi-constraint warping, the proposed method adopts a combination of disparity minimized homography and global homography, which can estimate a more accurate warping model and provide satisfactory image stitching results.

Similarly to CSPS, HWM uses disparity constraints to control disparity. The third row of Fig. 8(c) shows that HWM obtains a good stereoscopic image result with fewer vertical disparities. However, HWM may cause blur at the object boundary in overlapping regions. For example, the first two rows of Fig. 8(c) show that there are ghosts at the edge of the sculpture (see the enlarged red boxes in Fig. 8(c)). In contrast, our method obtains a sculpture with a clear boundary (see the first two rows in Fig. 8(d)). Owing to the disparity minimized homography and global warping are applied to warp the target images and reference image, respectively, our method provides accurate alignment and preserves the image content well.



Fig. 5. The comparison samples on the Flowerpot image between APAP and the proposed method. From top to bottom: left images, right images, and red-cyan anaglyph of stereoscopic images.

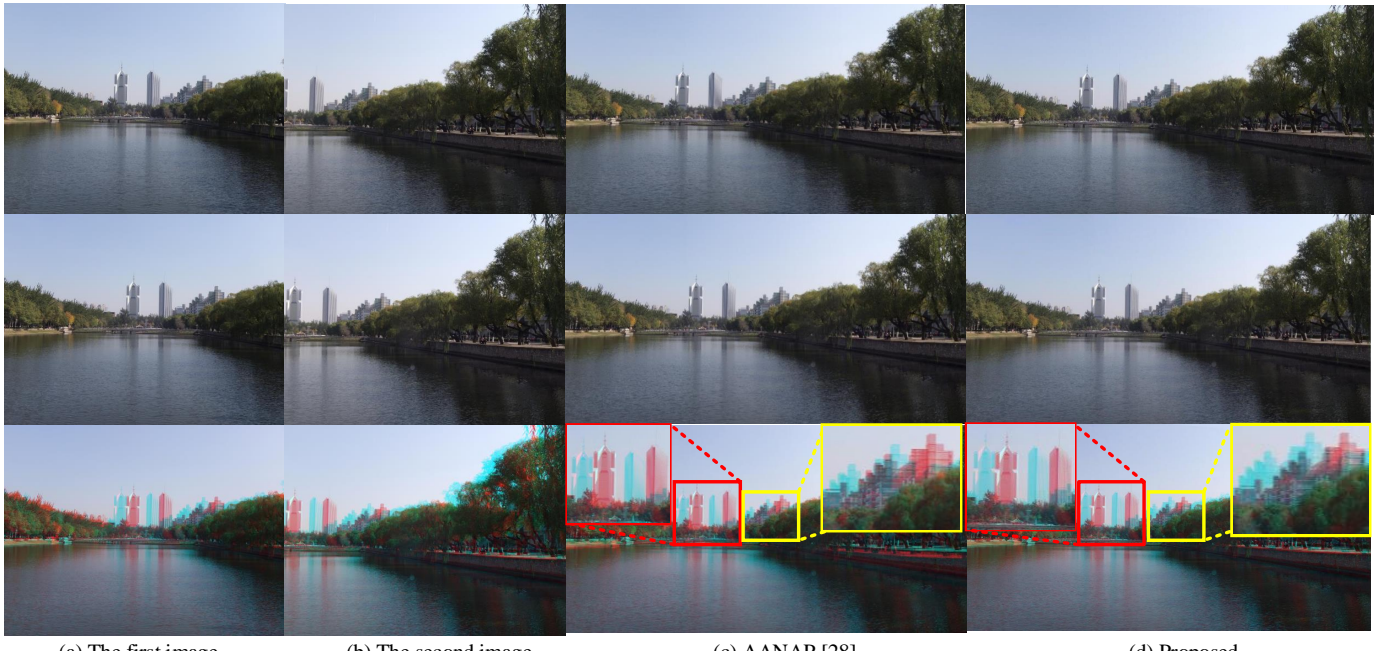


Fig. 6. The comparison samples on the Lake image between AANAP and the proposed method. From top to bottom: left images, right images, and red-cyan anaglyph of stereoscopic image.

**2) Quantitative Comparison:** To evaluate the performance of different image stitching approaches quantitatively, AVD and AG are utilized for performance comparison in this section. The AVD values of the final stereoscopic images from different methods are shown in Table I and 10 test samples (left images) are shown in Fig. 9. It is worth noting, for the 6 stereoscopic images in the second dataset [43], the AVD values of CSPS and HWM are obtained from the study [43]. It can be seen that the AVD values of the proposed method are smaller than those of APAP and AANAP, which demonstrates the effectiveness of the disparity constraint in stereoscopic image stitching. Furthermore, CSPS and HWM perform worse in p-

reserving disparity consistency than the proposed method. This is because both methods suffer from shape distortion, which produces the undesired vertical disparity. Benefiting from the combination of a disparity constraint and image warping, the proposed method is superior in stitching stereoscopic images.

The mean AG values of the final stitched left and right images from different methods are reported in Table II. It can be seen that APAP and AANAP cannot completely obtain high-quality stitched images, because these two methods do not consider the disparity constraint in stereoscopic image alignment. The proposed method works better than CSPS and HWM in preserving image content structures, since the

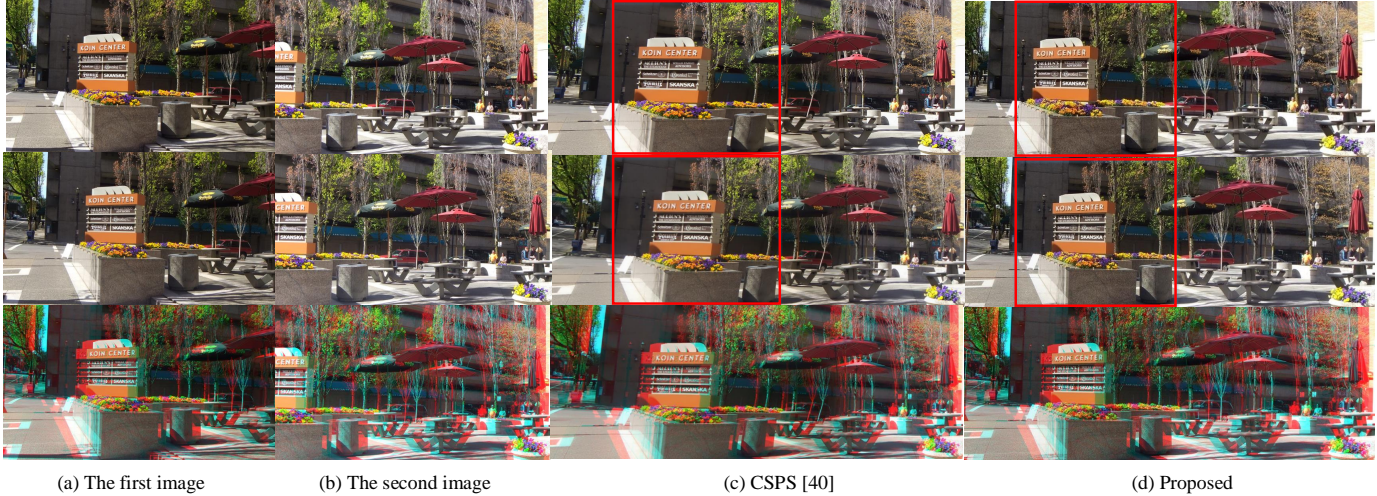


Fig. 7. The comparison samples on the Umbrella image between CSPS and the proposed method. From top to bottom: left images, right images, and red-cyan anaglyph of stereoscopic images.

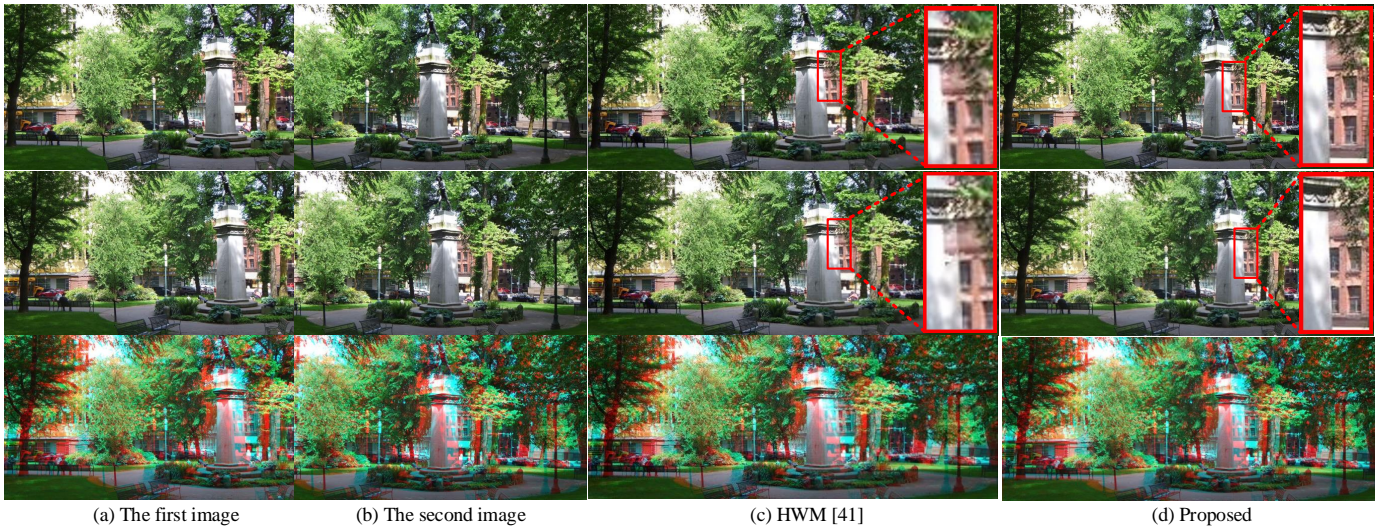


Fig. 8. The comparison samples on the Sculpture image between HWM and the proposed method. From top to bottom: left images, right images, and red-cyan anaglyph of stereoscopic image.

proposed method is flexible to warp and blend the left and right images according to the disparity map. The comparison shows the proposed method can not only preserve the disparity consistency of the stereoscopic image but also eliminate ghosts.

TABLE I  
AVERAGE VERTICAL DISPARITY(/PIXEL)

Datasets	APAP	AANAP	CSPS	HWM	Proposed
Flowerpot	1.10	1.13	0.88	<b>0.84</b>	<b>0.69</b>
House	1.09	1.10	0.79	<b>0.73</b>	<b>0.72</b>
Umbrella	1.15	1.16	0.77	<b>0.62</b>	<b>0.56</b>
Sculpture	1.40	1.08	0.74	<b>0.61</b>	<b>0.60</b>
Lake	2.69	2.55	0.92	<b>0.90</b>	<b>0.85</b>
Office Building	1.19	1.25	<b>1.09</b>	<b>1.03</b>	1.15
Alocasia	6.37	3.42	1.26	<b>2.21</b>	<b>1.13</b>
White Building	2.80	2.59	<b>1.35</b>	1.36	<b>1.21</b>
Flower	2.56	2.99	1.13	<b>1.08</b>	<b>1.10</b>
Panorama	2.81	2.71	1.40	<b>1.39</b>	<b>1.25</b>

TABLE II  
AVERAGE GRADINET(/PIXEL)

Datasets	APAP	AANAP	CSPS	HWM	Proposed
Flowerpot	6.96	5.75	7.07	<b>7.58</b>	<b>9.39</b>
House	7.26	7.37	8.35	<b>9.43</b>	<b>9.60</b>
Umbrella	7.34	9.47	<b>13.17</b>	12.52	<b>13.45</b>
Sculpture	11.93	13.99	16.96	<b>17.06</b>	<b>17.98</b>

### C. Evaluation of Key Components

In this section, we evaluate the importance of the disparity constraints of three key components of the proposed method, namely pre-aligning with disparity minimized homography (PDMH), multi-constraint warping based alignment (MCWA), and disparity consistency seam-cutting and blending (DCSB). To investigate how each component contributes to the stereoscopic image stitching, two quantitative comparison metrics (AVD and AG) are conducted on the first dataset [42]. Three variants of the proposed method are implemented as follows.

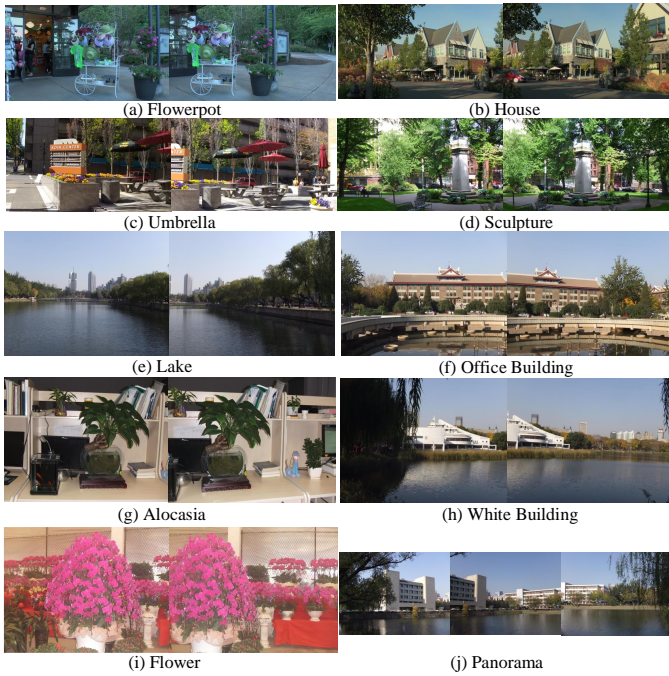


Fig. 9. Ten test samples (left images) used in quantitative comparison.

Variant 1: we remove the disparity constraint in PDMH to evaluate its effectiveness. Specifically, we use PDMH without a disparity constraint for pre-aligning the image and keeping the MCWA and DCSB processes to remain the same. Variant 2: we remove the disparity constraint in MCWA to evaluate its effectiveness. Specifically, we use MCWA without a disparity constraint for aligning the image and keeping the PDMH and DCSB processes to remain the same. Variant 3: we remove the disparity constraint in DCSB. Specifically, we use DCSB without a disparity constraint for blending the image and keeping the PDMH and MCWA processes to remain the same.

The quantitative comparison results of AVD are shown in Table III. It can be seen from the table that the proposed method outperforms the other three cases, which illustrates that the disparity constraint plays an essential role in reducing the vertical disparity of the stereoscopic image. In other words, the proposed method can preserve the disparity consistency of stereoscopic images and provide a better 3D viewing experience than the other cases. Table IV presents the quantitative comparison results of AG. The proposed method provides a lower geometric error and yields better stitching accuracy than the other cases, which validates that the disparity constraint can help obtain a high-quality stereoscopic image by preserving image structure and perspective.

TABLE III  
QUANTITATIVE COMPARISONS OF AVERAGE VERTICAL DISPARITY BETWEEN DIFFERENT VARIANTS(/PIXEL)

Datasets	Variant 1	Variant 2	Variant 3	Proposed
Flowerpot	0.85	0.95	0.89	0.69
House	0.89	0.92	0.90	0.72
Umbrella	0.78	0.85	0.74	0.56
Sculpture	0.75	0.87	0.63	0.60

TABLE IV  
QUANTITATIVE COMPARISONS OF AVERAGE GRADINET BETWEEN DIFFERENT VARIANTS(/PIXEL)

Datasets	Variant 1	Variant 2	Variant 3	Proposed
Flowerpot	7.45	8.25	7.98	9.39
House	5.54	7.34	9.12	9.60
Umbrella	8.45	10.45	11.40	13.45
Sculpture	12.78	13.24	14.71	17.98

#### D. Computing Complexity and Discussions

To demonstrate the efficiency of the proposed method, the computational complexity is discussed in this section. The proposed method is implemented in MATLAB R2016a, and the experiments are performed on the Windows 7 Operating System on an Intel Core i7-7700M Quad Core Processor CPU with 4 GB 3.60 GHz RAM. For the left “Sculpture” image, with a resolution of  $1000 \times 563$ , our method takes 6.36 s to generate the final left image stitching result. As a comparison, APAP takes 0.54 s and AANAP costs 3.5 s. Our method performs multi-constraint warping based alignment, and thus has higher computational complexity. However, it is worth spending the time to obtain a high-quality stitched result. In the future, we would like to speed up our scheme by using parallel computing to obtain real-time performance, which is critical for virtual reality applications.

## V. CONCLUSION

In this paper, a stereoscopic image stitching method via disparity-constrained warping and blending is presented. In the pre-alignment process, a disparity minimized homography is introduced to pre-align left and right images and mitigate the vertical disparity of a stereoscopic image. In the alignment process, a multi-constraint warping energy function is designed to fine-tune image warping, and the an initial disparity map is adopted to preserve disparity consistency. Finally, a disparity consistency seam-cutting and blending method is developed to determine a high-quality seam for image blending. The comprehensive experimental results illustrate the effectiveness of the proposed stereoscopic image stitching method.

## REFERENCES

- [1] J. Yang, X. Ye, K. Li, C. Hou, and Y. Wang, “Color-guided depth recovery from RGB-D data using an adaptive autoregressive model,” *IEEE Transactions on Image Processing*, vol. 23, no. 8, pp. 3443-3458, 2014.
- [2] H. Yuan, S. Kwong, J. Liu, and J. Sun, “A novel distortion model and lagrangian multiplier for depth maps coding,” *IEEE Transactions on Circuits and Systems for Video Technology*, vol. 24, no. 3, pp. 443-451, 2014.
- [3] J. Lei, J. Duan, F. Wu, N. Ling and C. Hou, ”Fast mode decision based on grayscale similarity and inter-view correlation for depth map coding in 3D-HEVC,” *IEEE Transactions on Circuits and Systems for Video Technology*, vol. 28, no. 3, pp.706-718, 2018.
- [4] A. J. Wagenmaker, B. E. Moore, R. R. Nadakuditi, “Robust photometric stereo using learned image and gradient dictionaries,” *IEEE International Conference on Image Processing (ICIP)*, Beijing, China, Sept. 2017, pp. 1457-1461.
- [5] J. Lei, C. Zhang, Y. Fang, Z. Gu, N. Ling, and C. Hou, “Depth sensation enhancement for multiple virtual view rendering,” *IEEE Transactions on Multimedia*, vol. 17, no. 4, pp. 457-469, 2015.

- [6] Y. Fang, C. Zhang, H. Huang, and J. Lei, "Visual attention prediction for stereoscopic video by multi-module fully convolutional network," *IEEE Transactions on Image Processing*, DOI: 10.1109/TIP.2019.2916766, 2019.
- [7] Y. Weng, W. Xu, Y. Wu, K. Zhou, and B. Guo, "2D shape deformation using nonlinear least squares optimization," *Visual Computer*, vol. 22, no. 9-11, pp. 653-660, 2006.
- [8] A. Eden, M. Uyttendaele, and R. Szeliski, "Seamless image stitching of scenes with large motions and exposure differences," *IEEE Computer Society Conference on Computer Vision and Pattern Recognition (CVPR'06)*, New York, NY, USA, June 2006, pp. 2498-2505.
- [9] Q. Chai, S. Liu, "Shape-optimizing hybrid warping for image stitching," *IEEE International Conference on Multimedia and Expo (ICME)*, Seattle, WA, USA, July 2016, pp. 1-6.
- [10] B. Xu, Y. Jia, "Wide-angle image stitching using multi-homography warping," *IEEE International Conference on Image Processing (ICIP)*, Beijing, China, Sept. 2017, pp. 1467-1471.
- [11] F. Bellavia, and C. Colombo, "Dissecting and reassembling color correction algorithms for image stitching," *IEEE Transactions on Image Processing*, vol. 27, no. 2, pp. 735-748, 2018.
- [12] J. Li, Z. Wang, S. Lai, Y. Zhai, and M. Zhang, "Parallax-tolerant image stitching based on robust elastic warping," *IEEE Transactions on Multimedia*, vol. 20, no. 7, pp. 1672-1687, 2018.
- [13] J. Lei, B. Peng, C. Zhang, X. Mei, X. Cao, X. Fan, X. Li, "Shape-preserving object depth control for stereoscopic images," *IEEE Transactions on Circuits and Systems for Video Technology*, DOI: 10.1109/TCSVT.2017.2749146, 2017.
- [14] F. Zhang and F. Liu, "Parallax-tolerant image stitching," *IEEE Conference on Computer Vision and Pattern Recognition*, Columbus, OH, USA, June 2014, pp. 3262-3269.
- [15] L. E. Gurrieri, and E. Dubois, "Stereoscopic cameras for the realtime acquisition of panoramic 3D images and videos," *Proc. SPIE 8648, Stereoscopic Displays and Applications XXIV*, vol. 8648, pp. 1-17, 2013.
- [16] J. Yang, Z. Gan, K. Li, and C. Hou, "Graph-based segmentation for RGB-D data using 3-D feometry enhanced superpixels," *IEEE Transactions on Cybernetics*, vol. 45, no. 5, pp. 927-940, 2015.
- [17] H. Tang, and Z. Zhu, "Content-based 3-D mosaics for representing videos of dynamic urban scenes," *IEEE Transactions on Circuits and Systems for Video Technology*, vol. 22, no. 2, pp. 295-308, 2012.
- [18] C. Richardt, Y. Pritch, H. Zimmer, A. S-Hornung, "Megastereo: constructing high-resolution stereo panoramas," *IEEE Conference on Computer Vision and Pattern Recognition*, Portland, OR, USA, June 2013, pp. 1256-1263.
- [19] S. Peleg, M. B-Ezra, and Y. Pritch, "Omnistereo: panoramic stereo imaging," *IEEE Transactions on Pattern Analysis and Machine Intelligence*, vol. 23, no. 3, pp. 279-290, 2001.
- [20] N. Li, Y. Xu, and C. Wang, "Quasi-homography warps in image stitching," *IEEE Transactions on Multimedia*, vol. 20, no. 6, pp. 1365-1375, 2018.
- [21] C. Li, Z-Y. Liu, X. Yang, H. Qiao, J-H. Su, "Stitching contaminated images," *Neurocomputing*, vol. 214, pp. 829-836, 2016.
- [22] R. Szeliski, "Image alignment and stitching: a tutorial," *Foundations and Trends in Computer Graphics and Vision*, vol. 2, no. 1, pp. 1-104, 2006.
- [23] M. Brown and D. G. Lowe, "Recognising panoramas," *IEEE International Conference on Computer Vision*, Nice, France, France, Oct. 2003, pp. 1218-1225.
- [24] M. Brown and D. Lowe, "Automatic panoramic image stitching using invariant features," *International Journal of Computer Vision*, vol. 74, no. 1, pp. 59-73, 2007.
- [25] J. Gao, S. J. Kim, M. S. Brown, "Constructing image panoramas using dual-homography warping," *IEEE Conference on Computer Vision and Pattern Recognition*, Colorado Springs, CO, USA, June 2011, pp. 49-56.
- [26] W-Y. Lin, S. Liu, Y. Matsushita, T-T. Ng, L-F. Cheong, "Smoothly varying affine stitching," *IEEE Conference on Computer Vision and Pattern Recognition*, Colorado Springs, CO, USA, June 2011, pp. 345-352.
- [27] J. Zaragoza, T-J. Chin, M. S. Brown, D. Suter, "As-projective-as-possible image stitching with moving DLT," *IEEE Conference on Computer Vision and Pattern Recognition*, vol. 36, no. 7, pp. 2339-2346, 2014.
- [28] K. Joo, N. Kim, T-H. Oh, I. S. Kweon, "Line meets as-projective-as-possible image stitching with moving DLT," *IEEE International Conference on Image Processing (ICIP)*, Quebec City, QC, Canada, Sept. 2015, pp. 1175-1179.
- [29] C.-H. Chang, Y. Sato, Y.-Y. Chuang, "Shape-preserving half-projective warps for image stitching," *IEEE Conference on Computer Vision and Pattern Recognition*, Columbus, OH, USA, June 2014, pp. 3254-3261.
- [30] C.-C. Lin, S. U. Pankanti, K. N. Ramamurthy, and A. Y. Aravkin, "Adaptive as-natural-as-possible image stitching," *IEEE Conference on Computer Vision and Pattern Recognition (CVPR)*, Boston, MA, USA, June 2015, pp. 1155-1163.
- [31] F. Liu, M. Gleicher, H. Jin, A. Agarwala, "Content preserving warps for 3d video stabilization," *ACM Transactions on Graphics*, vol. 28, no. 3, pp. 44:1-44:9, 2009.
- [32] W. Jiang, J. Gu, "Video stitching with spatial-temporal content-preserving warping," *IEEE Conference on Computer Vision and Pattern Recognition Workshops (CVPRW)*, Boston, MA, USA, June 2015, pp. 42-48.
- [33] Y.-S. Chen, and Y.-Y. Chuang, "Natural image stitching with the global similarity prior," *European Conference on Computer Vision*, Springer, Cham, 2016, pp. 186-201.
- [34] J. Hu, D.-Q. Zhang, H. Yu, C. Chen, "Multi-objective content preserving warping for image stitching," *IEEE International Conference on Multimedia and Expo (ICME)*, Turin, Italy, July 2015, pp. 1-6.
- [35] E. Dubrofsky, R. J. Woodham, "Combining Line and Point correspondences for homography estimation," *International Symposium on Visual Computing*, Springer, Berlin, Heidelberg, 2011, pp. 202-213.
- [36] T. Xiang, G.-S. Xia, L. Zhang, and N. Huang, "Locally warping-based image stitching by imposing line constraints," *International Conference on Pattern Recognition (ICPR)*, Cancun, Dec. 2016, pp. 4178-4183.
- [37] Y. Fang, Z. Chen, W. Lin, and C.-W. Lin, "Saliency detection in the compressed domain for adaptive image retargeting," *IEEE Transactions on Image Processing*, vol. 21, no. 9, pp. 3888-3901, 2012.
- [38] Z. Wang, X. Chen, and D. Zou, "Copy and paste: temporally consistent stereoscopic video blending," *IEEE Transactions on Circuits and Systems for Video Technology*, DOI: 10.1109/TCSVT.2017.2706197, 2017.
- [39] A. Buades and G. Facciolo, "Reliable multiscale and multiwindow stereo matching," *Siam Journal on Imaging Sciences*, vol. 8, no. 2, pp. 888-915, 2015.
- [40] K. Lin, N. Jiang, L.-F. Cheong, M. Do, and J. Lu, "SEAGULL: Seam-guided local alignment for disparity-tolerant Image Stitching," *European Conference on Computer Vision (ECCV)*, Springer, Cham, Oct. 2016, pp. 370-385.
- [41] N. Li, T. Liao, and C. Wang, "Perception-based energy functions in seam-cutting," *Signal Image and Video Processing*, vol. 12, no. 5, pp. 1-8, 2018.
- [42] F. Zhang and F. Liu, "Casual stereoscopic panorama stitching," *IEEE Conference on Computer Vision and Pattern Recognition (CVPR)*, Boston, MA, USA, June 2015, pp. 2002-2010.
- [43] W. Yan, C. Hou, J. Lei, Y. Fang, Z. Gu, and N. Ling, "Stereoscopic image stitching based on a hybrid warping model," *IEEE Transactions on Circuits and Systems for Video Technology*, vol. 27, no. 9, pp. 1934-1946, 2017.
- [44] D. G. Lowe, "Distinctive image features scale-invariant keypoints," *International Journal of Computer Vision*, vol. 60, no. 2, pp. 91-110, 2004.
- [45] S. Li, L. Yuan, J. Sun, L. Quan, "Dual-feature warping-based motion model estimation," *IEEE International Conference on Computer Vision*, Santiago, Chile, Dec. 2015, pp. 4283-4291.
- [46] P. F. Felzenszwalb and D.P. Huttenlocher, "Efficient graph-based image segmentation," *International Journal of Computer Vision*, vol. 59, no. 2, pp. 167-181, 2004.
- [47] C. Allene, J.-P. Pons, and R. Keriven, "Seamless image-based texture atlases using multi-band blending," *International Conference on Pattern Recognition*, Tampa, FL, USA, Dec. 2008, pp. 1-4.
- [48] T. Plotz, S. Roth, "Registering images to untextured geometry using average shading gradients," *IEEE International Conference on Computer Vision (ICCV)*, Santiago, Chile, Dec. 2016, pp. 2030-2038.



**Xiaoting Fan** received the M.S. degree from the Xi'an Polytechnic University, Xi'an, Shaanxi, China, in 2017. She is currently pursuing the Ph.D. degree with the School of Electrical and Information Engineering, Tianjin University, Tianjin, China.

She was a visiting student at the School of Computer Science and Engineering, Nanyang Technological University, Singapore, from December 2018 to March 2019. Her research interests include 3D image processing, virtual reality and computer vision.



**Jianjun Lei** (M'11-SM'17) received the Ph.D. degree in signal and information processing from Beijing University of Posts and Telecommunications, Beijing, China, in 2007.

He was a visiting researcher at the Department of Electrical Engineering, University of Washington, Seattle, WA, from August 2012 to August 2013. He is currently a Professor at Tianjin University, Tianjin, China. His research interests include 3D video processing, virtual reality, and artificial intelligence.



**Nam Ling** (S'88-M'90-SM'99-F'08) received the B.Eng. degree from the National University of Singapore, Singapore, in 1981, and the M.S. and Ph.D. degrees from the University of Louisiana, Lafayette, LA, USA, in 1985 and 1989, respectively.

From 2002 to 2010, he was an Associate Dean with the School of Engineering, Santa Clara University, Santa Clara, CA, USA. He is currently the Sanfilippo Family Chair Professor and the Chair for the Department of Computer Engineering, Santa Clara University. He is also a Consulting Professor with

the National University of Singapore, a Guest Professor for Tianjin University, Tianjin, China, a Guest Professor for Shanghai Jiao Tong University, Shanghai, China, a Cuiying Chair Professor for Lanzhou University, Gansu, China, and a Distinguished Professor for Xian University of Posts and Telecommunications, Shaanxi, China. He has authored or coauthored over 180 publications and standard contributions, including two books in the fields of video coding and systolic arrays. He has filed/granted over 15 U.S. patents.

Dr. Ling is an IEEE Fellow due to his contributions to video coding algorithms and architectures. He is also an IET Fellow. He was named as an IEEE Distinguished Lecturer twice and was also an APSIPA Distinguished Lecturer. He received the IEEE ICCE Best Paper Award (First Place). He was a recipient of six awards from Santa Clara University, four at the University level (Outstanding Achievement, Recent Achievement in Scholarship, Presidents Recognition, and Sustained Excellence in Scholarship) and two at the School/College level (Researcher of the Year and Teaching Excellence). He was a Keynote Speaker for IEEE APCCAS, VCVP (twice), JCPC, IEEE ICAST, IEEE ICIEA, IET FC Umedia, IEEE Umedia, and Workshop at XUPT, as well as a Distinguished Speaker for IEEE ICIEA. He has served as a General Chair/Co-Chair for IEEE Hot Chips, VCVP (twice), IEEE ICME, IEEE Umedia (thrice), and IEEE SiPS. He has also served as a Technical Program Co-Chair for IEEE ISCAS, APSIPA ASC, IEEE APCCAS, IEEE SiPS (twice), DCV, and IEEE VCIP. He was a Technical Committee Chair for IEEE CASCOM TC and IEEE TCMM, and has served as a Guest Editor or Associate Editor for the IEEE TRANSACTIONS ON CIRCUITS AND SYSTEMSII: REGULAR PAPERS, the IEEE JOURNAL OF SELECTED TOPICS IN SIGNAL PROCESSING, Springer JSPS, Springer MSSP, and more.



**Yuming Fang** (M'13-SM'17) received his Ph.D. degree from Nanyang Technological University in Singapore, M.S. degree from Beijing University of Technology in Beijing, China, and B.E. degree from Sichuan University in Chengdu, China. Currently, He is a Professor in the School of Information Management, Jiangxi University of Finance and Economics, Nanchang, China. He serves as an Associate Editor of IEEE Access and is on the editorial board of Signal Processing: Image Communication. His research interests include visual attention modeling,

visual quality assessment, computer vision, 3D image/video processing, etc.



**Qingming Huang** (SM'08-F'18) is a professor in the University of Chinese Academy of Sciences and an adjunct research professor in the Institute of Computing Technology, Chinese Academy of Sciences. He graduated with a Bachelor degree in Computer Science in 1988 and Ph.D. degree in Computer Engineering in 1994, both from Harbin Institute of Technology, China.

His research areas include multimedia video analysis, image processing, computer vision and pattern recognition. He has published more than 400 academic papers in prestigious international journals including IEEE Trans. Image Process., IEEE Trans. Multimedia, IEEE Trans. Circuits Syst. Video Technol., etc., and top-level conferences such as ACM Multimedia, ICCV, CVPR, IJCAI, VLDB, etc. He is the associate editor of IEEE Trans. Circuits Syst. Video Technol., and Acta Automatica Sinica, and the reviewer of various international journals including IEEE Trans. Multimedia, IEEE Trans. Circuits Syst. Video Technol., IEEE Trans. Image Process., etc. He is a Fellow of IEEE and has served as general chair, program chair, track chair and TPC member for various conferences, including ACM Multimedia, CVPR, ICCV, ICME, PCM, PSIVT, etc.



**Chunping Hou** received the M.Eng. and Ph.D. degrees, both in electronic engineering, from Tianjin University, Tianjin, China, in 1986 and 1998, respectively.

Since 1986, she has been the faculty of the School of Electronic and Information Engineering, Tianjin University, where she is currently a Full Professor and the Director of the Broadband Wireless Communications and 3D Imaging Institute. Her current research interests include 3D image processing, 3D display, wireless communication, and the design and applications of communication systems.